33RD INTERNATIONAL COSMIC RAY CONFERENCE, RIO DE JANEIRO 2013
THE ASTROPARTICLE PHYSICS CONFERENCE

ICRC 2013

Acceleration of cosmic rays by young core-collapse supernova remnants.

I. TELEZHINSKY[1,2], V.V. DWARKADAS[3], M. POHL[1,2], R. BROSE[1], A. WILHELM[1,2]

[1] *DESY, Platanenallee 6, 15738 Zeuthen, Germany*
[2] *University of Potsdam, Institute of Physics & Astronomy, Karl-Liebknecht-Strasse 24/25, 14476 Potsdam, Germany*
[3] *University of Chicago, Department of Astronomy&Astrophysics, 5640 S Ellis Ave, AAC 010c, Chicago, IL 60637, U.S.A.*

igor.telezhinsky@desy.de

Abstract: Supernova remnants (SNRs) are thought to be the primary candidates for the sources of Galactic cosmic rays. According to diffusive shock acceleration theory, SNR shocks produce a power-law spectrum with an index of s = 2, perhaps non-linearly modified to harder spectra at high energy. Observations of SNRs often indicate particle spectra that are softer than that and show features not expected from classical theory. Known drawbacks of the standard approach are the assumption that SNRs evolve in a uniform environment, and that the reverse shock does not accelerate particles. Relaxing these assumptions increases the complexity of the problem, because one needs reliable hydrodynamical data for the plasma flow as well as good estimates for the magnetic field at the reverse shock. We show that these two factors are especially important when modeling young core-collapse SNRs that evolve in a complicated circumstellar medium shaped by the winds of progenitor stars. We use high-resolution numerical simulations for the hydrodynamical evolution of the SNR. Instead of parametrizations of the magnetic-field profiles inside the SNR, we follow the advection of frozen-in magnetic field inside the SNR, and thus obtain the B-field value at all locations, in particular at the reverse shock. To model cosmic-ray acceleration we solve the cosmic-ray transport equation in test-particle approximation. We find that the complex plasma-flow profiles of core-collapse SNRs significantly modify the particle spectra. Additionally, the reverse shock strongly affects the emission spectra and the surface brightness. We also show first results of studies that include self-consistent growth, transport, and decay of magnetic turbulence.

Keywords: supernova remnants, cosmic rays, magnetic field, hydrodynamics

1 Introduction

The theory of diffusive shock acceleration (DSA) [1, 2, 3, 4] applied to supernova remnants (SNRs) suggests that particle spectra should follow a power-law with index, $s = 2$, and an exponential cut-off at very high energy. However, recent observational data on, e.g., RX J0852.0-4622 [5], RCW 86 [6], SN 1006 [7], Cas A [8, 10], and Tycho's SNR [9, 11] indicate that the particle spectra are significantly softer. Moreover, the spectral shape is not a pure power law with exponential cut-off, as for example in Cas A. Several groups have introduced modifications to DSA theory to account for partially neutral medium in the forward shock (FS) vicinity [12, 13], Alfvénic drift of scattering centers [14, 15], turbulent shock [16], or multiple weak secondary shocks that appear when the FS propagates through a medium filled with small dense cloudlets [17].

The largest and strongest secondary shock in the system is the reverse shock (RS) that propagates through the ejecta. High-resolution radio and X-ray observations support the notion that particle acceleration can also occur at the RS [18, 19, 20, 21, 22], but only recently has this possibility been considered in theoretical calculations [23, 24, 25, 26]. The RS accelerates particles of the ejecta and thus provides a second population of relativistic particles in addition to that produced at the FS, a critical parameter for which is the magnetic field (MF) at the RS. The superposition of these two components may lead to significant spectral modifications in the volume-integrated emission from SNRs. Another recent step forward is an account for a realistic hydrodynamical profile of the circumstellar medium (CSM) in recent calculations [28, 24, 29, 26].

Here we show that the acceleration of particles at the RS and the complex hydrodynamics of SNRs are both important for modeling young core-collapse SNRs. The resulting volume-integrated spectrum of particles and their consequent radiation is significantly different from that of planar-shock calculations and dependent on the type of SNR. To accomplish our study, we perform high-resolution simulations of the hydrodynamical evolution of SNR with initial and environmental conditions representative of type Ic and type IIP supernovae (SNe). We consider the transport of frozen-in MF by the plasma flow inside the SNR to trace its evolution inside the remnant, particularly in the RS region, separately for the radial and the tangential field. We model cosmic-ray acceleration by solving the cosmic-ray transport equation in test-particle approximation. Finally, we calculate the resulting emission from the SNR and construct surface-brightness maps in various energy bands.

2 Method

For a detailed description of the method a reader is referred to our earlier work [27]. Here we give a brief outline.

2.1 Hydrodynamics

We investigate type Ic and type IIP SNe, because they arise from different types of progenitors, Wolf-Rayet (WR) and Red Supergiants (RSGs) respectively, with considerably different wind velocities leading to a large variation in the ambient medium into which the SNR expands, and because many SNe, even those of other types, will fall somewhere close to or in between these types. As a star

moves off the main sequence into the RSG stage, it grows considerably in size, the wind mass-loss rate increases to about $5\times10^{-5}M_{\odot}\mathrm{yr}^{-1}$ while the velocity drops to a low value of about 10 km s^{-1}. This results in a new pressure equilibrium. The high density ($\propto \dot{M}/v_w$) of the RSG wind leads to the formation of a wind region with density almost four orders of magnitude above that of the main-sequence wind.

Progenitors of type Ic SNe are WR stars, whose mass-loss rates are somewhat lower than those of RSG winds. Their wind velocities are more than two orders of magnitude higher, though, leading to correspondingly lower wind densities. The high momentum of the winds pushes outward on the RSG shell, breaking it up in the process and mixing its material into the WR wind [32]. This mixed material approaches the main-sequence shell, and eventually the system reaches an equilibrium situation that in many ways resembles the main-sequence bubble.

In each case we assumed an ejecta mass of about 5 $M_{\odot}$ and an explosion energy of 10^{51} ergs. The ejecta density is flat where the flow velocity is below a certain value, u_{fl}, and decreases as a power law with radius, $\rho_{ej}\propto r^{-9}$, where the flow velocity is above u_{fl} [30, 31]. The interaction of the ejecta with the wind medium sets up a double-shock structure as expected, consisting of a FS and RS separated by a contact discontinuity (CD).

The shock expansion in the wind medium in both cases is initially quite similar. The evolution changes and is no longer self-similar, once the FS reaches the end of the freely expanding wind region. In the RSG case one finds a huge drop in density beyond the wind region, whereas in the WR case one finds an increase in density by a factor of 4. The interaction of the FS with the wind termination shock leads to a reflected shock that travels back into the ejecta in the case of the type Ic SN. In the case of the type IIP, the steep drop leads to the formation of a complicated ejecta structure. These flow structures are used to compute the acceleration of particles at the shock fronts.

2.2 Magnetic field

The acceleration and subsequent radiation of relativistic particles significantly depends on the distribution of MF in the SNR, especially in the upstream and downstream vicinities of the shocks. We implemented a calculation of the MF inside SNRs, which is especially important for the acceleration of particles at the RS. We assume that the SNR is filled with a perfectly conducting fluid, in which case the magnetic field is frozen into the plasma and satisfies the induction equation

$$\frac{\partial \mathbf{B}}{\partial t} = \bigtriangledown \times (\mathbf{u}\times\mathbf{B}), \qquad (1)$$

where **B** is the MF and **u** is the flow speed. If the MF is dynamically unimportant, the solving Eq.1 on the hydrodynamical flow profile is equivalent to the full solution in ideal MHD. We assume that in the ejecta both the radial and the tangential field components are constant, where $u_r \le u_{fl}$, and scaling $1/r^2$ where $u_r > u_{fl}$. The amplitude is set so that the total volume-averaged MF strength is $\simeq 50$ G when $R_{\mathrm{SN}} = 10^{15}$ cm.

We limit ourselves to scenarios with no amplification of the MF upstream of the FS, and only the CSM field is assumed to be transported through the shock. We assume that turbulence equalizes all components of the MF in the wind zones until they are transported through the FS. The radial profile of the MF in the environment of a core-collapse SNR in our description is then given by $B(r) = B_{\mathrm{st}}R_{\mathrm{st}}/r$ between the surface of the progenitor star at R_{st} ($\approx 8R_{\odot}$ for WR star, $\approx 600R_{\odot}$ for RSG) and R_{b}, the radius of the wind-blown bubble in our simulations (≈ 7 pc for WR star, ≈ 2 pc for RSG). Beyond R_{b} and out to the swept-up shell (≈ 30 pc in both cases), we assume a constant field strength, $B(R_{\mathrm{b}})\sqrt{11}$.

2.3 Cosmic-ray acceleration

For our time-dependent kinetic calculations in test-particle approximation [25, 26] we numerically solve the diffusion-advection equation for the differential particle number density on a grid co-moving with the shock wave and in spherically symmetric geometry. To resolve the diffusion length of the lowest energy particles, we performed a coordinate transformation that increases the spatial resolution near the shock. The spatial coordinate, x, is related to the new uniformly binned coordinate, x_*, as

$$(x-1) = (r/R_{\mathrm{SH}}-1) = (x_*-1)^3\,, \qquad (2)$$

where R_{SH} is the shock radius. Thus, with modest resolution in x_*, we achieve a very fine resolution in x where it matters, while an implicit algorithm permit using a moderately large timestep. The other benefit is a significant extension of the grid toward $x \gg 1$ at very low computational cost. The boundary condition for large x then does not really affect our solution, since particles do not leak out of the grid but rather are distributed over the huge upstream volume according to the diffusion properties of the media. We included an exponential transition from Bohmian to Galactic diffusion at around $2R_{\mathrm{FS}}$. A high Galactic diffusion coefficient also compensates for the low resolution of the spatial grid beyond $2R_{\mathrm{FS}}$. To maintain the validity of the test-particle approximation, we did not permit the CR pressure at the shock to exceed 10% of the ram pressure by adjusting the injection coefficient in a thermal-leakage model [33].

3 Particle spectra

We present at Fig. 1 snapshots at the age of 400, 1000, and 1975 years of particle spectra for type-Ic and type-IIP SNRs. We show spectra produced by acceleration at the FS and RS and the sum of both from the whole SNR.

At an age of 400 years the FSs of both SNR types are still propagating through the freely expanding stellar wind, and the spectra of protons accelerated by both the FS and the RS are consistent with standard DSA. The magnetic field at the RS is considerably smaller than at the FS, and so particles reach TeV energies only. In type-Ic SNR the number of particles injected into the acceleration process at the RS is larger than at the FS, therefore the CR contribution of the RS has a higher intensity. Since the MF is not strong enough at either of the shocks to cause significant synchrotron losses, the electron spectra look similar to those of protons. The bump in the electron spectra produced at the RS arises from extending the volume integral over both the up- and downstream region of the RS (see Section 5.1.1 of [25] for details).

At 1000 years, type-Ic SNR particle spectra produced by the FS differ significantly from standard DSA on account of the recent interaction of the FS with the wind ter-

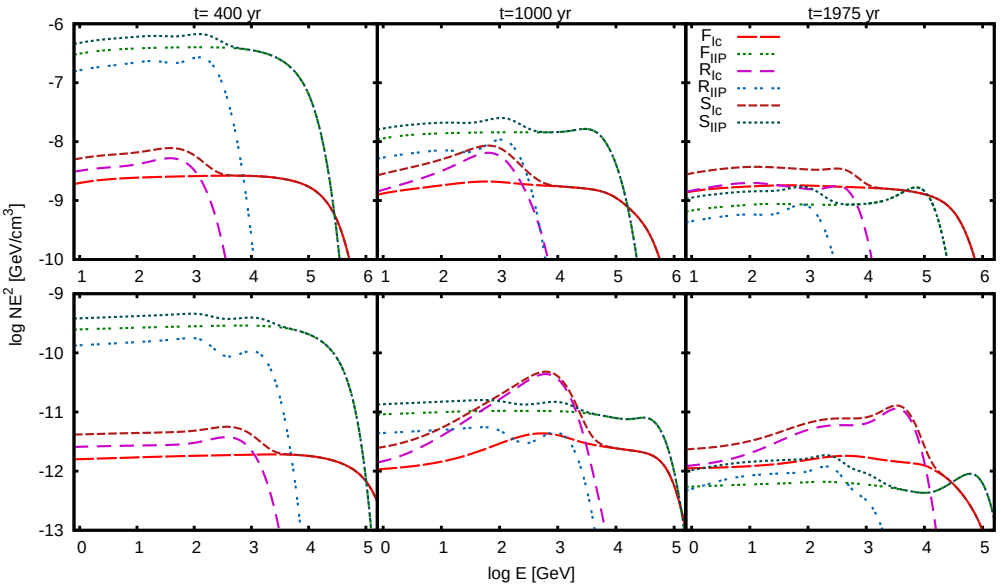

Figure 1: Time evolution of proton (top) and electron (bottom) spectra for type-Ic and type-IIP SNR. Total volume-integrated spectra (S) are the sum of the contributions from the forward (F) and reverse (R) shocks.

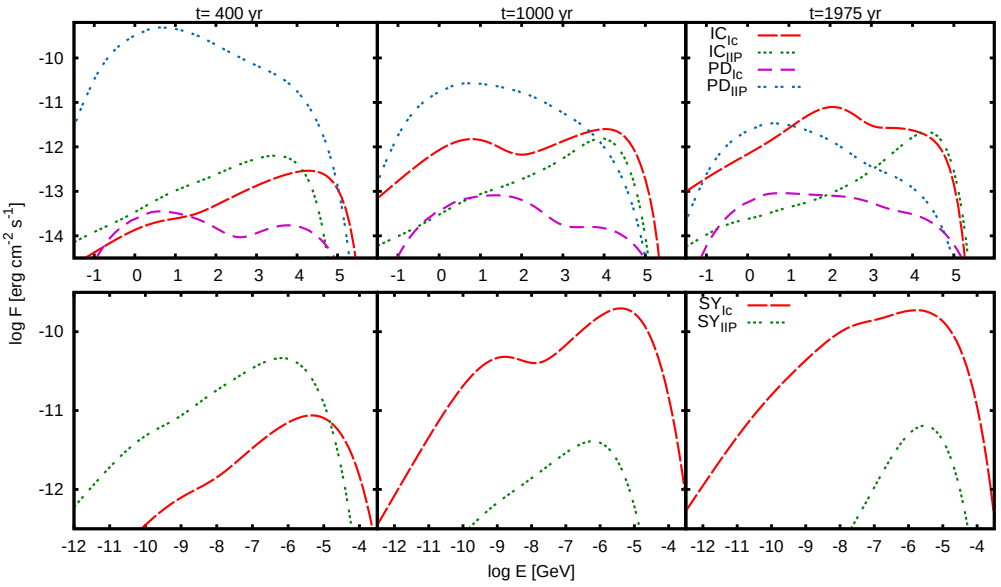

Figure 2: Time evolution of emission spectra from type-Ic and type-IIP SNRs due to pion-decay (PD), inverse Compton (IC) (both top panel), and synchrotron (SY) radiation (bottom panel).

mination shock that briefly boosted acceleration. By coincidence, the time when the reflected shock created in this interaction reached the RS is around 1000 years. So the RS spectra are rather specific for this particular time, but we show them to illustrate the impact of the hydrodynamics on particle spectra. Type-IIP SNRs do not show such a strong variation in particle spectra because the FS entered a very dilute environment, so no additional compression and acceleration occurred. The maximum energy of CRs increased as expected on account of increased velocity of the FS, but the rate of particle injection dropped drastically.

At the age of 1975 years, the velocity profiles of both remnant types have relaxed. The multiple weak reflected shocks in type-Ic SNR have dissipated, but the CR spectra still retain their effects, though in general they appear smoother than before. The proton distributions from both the FS and the RS are softer, and the contribution from the RS to the total proton spectra remains visible. The electrons accelerated by the FS have rather soft spectra as well, while those accelerated by the RS dominate the total electron spectra of type-Ic SNR. We see an excess of high-energy CRs accelerated at the FS of type-IIP SNR which is a signature of a delayed response to a sudden change in the injection rate. For the high-energy CRs the characteristic diffusion-advection timescale, $\tau_{\rm da} = \kappa/v_s^2$, is long, and therefore they continue to diffuse around the shock, while low-energy particles are quickly detached from the shock.

4 Nonthermal emission

We considered three radiation processes of non-thermal particles: synchrotron and inverse Compton (IC) emission

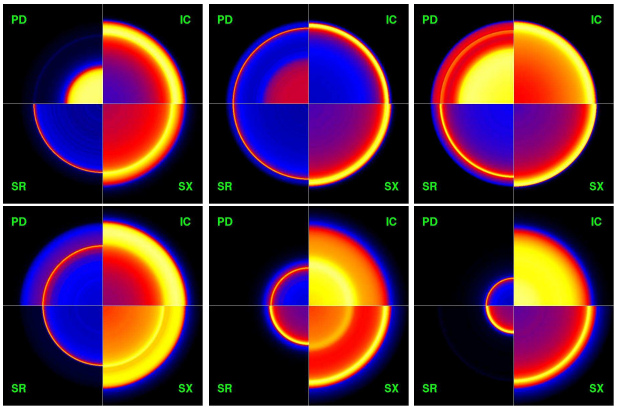

Figure 3: Time evolution of intensity maps of type-Ic (top) and type-IIP (bottom) SNRs at 1 TeV due to pion-decay (PD) and inverse Compton (IC), at 3 keV (SX) and at 1.4GHz (SR) due to synchrotron radiation. The left column is for the age of 400 years, the middle column at 1000 years, and the right column at 1975 years. The scale is linear from zero to maximum in each image. All images are scaled with the FS radius, $R_{FS}(t)$.

of electrons, and pion-decay emission following inelastic collisions of CR protons. Only primary electrons are considered for the leptonic processes. The calculated photon distributions for type-Ic SNR and type-IIP SNR are plotted at Fig. 2. We also calculate, and discuss in context with the radiation spectra, intensity maps at characteristic radio, X-ray and gamma-ray wavelengths, that are shown in Fig. 3. We note that in all calculations of volume-integrated spectra or intensity maps the radial distributions of CRs, the target material, and the MF are taken into account. The results are significantly different from those of simple toy-models that assume uniform particle, density, and MF profiles inside the SNR.

Emission spectra from core-collapse SNRs are complex, reflecting both the distribution of gas or MF and the spectral differences between the CRs coming from the FS and RS. High-energy emission from type-Ic SNR is dominated by leptonic processes, particularly so when the SNR is older. High-energy radiation from type-IIP SNRs is very soft and strongly dominated by pion-decay emission, except for late-stage emission at the highest energies.

Both types of remnants show, in addition to a shell structure, a center-filled morphology (see Fig. 3) of high-energy emission, because the dense and weakly magnetized ejecta in the interior permits high-energy particles to propagate and radiate there. The shell-type morphology of type-IIP SNR, however, may be difficult to resolve with the current generation of gamma-ray telescopes. The complex radial distribution of MF causes significant differences in the morphology of synchrotron and IC emission from core-collapse SNRs, and therefore a "re-mapping" of the spectra and morphology of the two types of leptonic emission is not advised.

5 Conclusions

Using realistic models for the circumstellar medium created by stellar mass-loss around massive stars, we have studied the hydrodynamical evolution of SNR and computed the acceleration, transport, and emission of CRs in them. We explicitly account for changes in mass-loss rate as the progenitor star evolved through various stages. The resulting density transitions, that characterize the circumstellar medium, induce a large modification in the particle spectra and the radiation signatures.

We advanced our model of particle acceleration and propagation in SNRs [25, 26] by adding realistic transport of the MF. Our calculations suggest that the MF at the RS is sufficient to accelerate particles to TeV energies. Although the maximum energy of cosmic rays at the RS is lower than at the FS, their intensity is high on account of the high ejecta density in core-collapse SNRs. Thus the RS contributes a significant fraction of the total CR intensity in SNRs at early times. The RS-accelerated particles soften the total emission spectra, in agreement with recent data, and affect the intensity distribution. The high-energy emission from type-Ic SNRs is initially roughly an order of magnitude fainter than that of type-IIP SNRs at early ages, but does not fade away as quickly , rendering type-Ic SNRs good targets for the current generation of telescopes.

Our work demonstrates that the hydrodynamics of SNRs and their interaction with the environment play a significant role in shaping particle and emission spectra as well as intensity maps. The emission from core-collapse SNRs is significantly different from that of type-Ia SNRs that evolve in a uniform environment [25].

Acknowledgment: We acknowledge support by the "Helmholtz Alliance for Astroparticle Physics HAP" funded by the Initiative and Networking Fund of the Helmholtz Association. VVD's work is supported by NASA Fermi grant NNX12A057G.

References

[1] W. I. Axford, et. al, ICRC Proc., 1977, 132-137.
[2] G. F. Krymskii, Ak.Sci. USSR Doklady 234, 1977, 1306.
[3] A. R. Bell, MNRAS 182, 1978, 147-156.
[4] R. D. Blandford, J. P. Ostriker, ApJL 221, 1978, L29-L32.
[5] F. Aharonian, et al., ApJ 661, 2007, 236-249.
[6] F. Aharonian, et al., ApJ 692, 2009, 1500-1505.
[7] F. Acero, et al. A&A 516, 2010, A62+.
[8] V. A. Acciari, et al., ApJ 714, 2010, 163-169.
[9] V. A. Acciari, et al., ApJL 730, 2011, L20.
[10] A. A. Abdo, et al., ApJL 710, 2010, L92-L97.
[11] F. Giordano, et al., ApJL 744, 2012, L2.
[12] M. Malkov, et al., Physics of Plasmas 19, 2012, 082901
[13] P. Blasi, et al., ApJ 755, 2012, 121
[14] V.N. Zirakashvili, V.S. Ptuskin, AIP 1085, 2008, 336-339.
[15] D. Caprioli, JCAP 7, 2012, 38.
[16] I. Lerche, et al., J. of Plasma Physics 64, 2000, 459-474.
[17] T. Inoue, et al., ApJL 723, 2010, L108-L112.
[18] E. Gotthelf, et. al., ApJL 552, 2001, L39-L43.
[19] J. Rho, et al., ApJ 581, 2002, 1116-1131.
[20] T. DeLaney, et al., ApJ 580, 2002, 914-927.
[21] M. Sasaki, et al., ApJ 642, 2006, 260-269.
[22] E. Helder, J. Vink., ApJ 686, 2008, 1094-1102.
[23] V.N. Zirakashvili, F.A. Aharonian, ApJ 708, 2010, 965-980.
[24] V.N. Zirakashvili, V.S. Ptuskin, APh 39, 2012, 12-21.
[25] I. Telezhinsky, et al., APh 35, 2012, 300-311.
[26] I. Telezhinsky, et al., A&A 541, 2012, A153.
[27] I. Telezhinsky, et al., A&A 552, 2013, A102.
[28] D. Ellison, A. Bykov, ApJ 731, 2011, 87+.
[29] D. Ellison, et al., ApJ 744, 2012, 39.
[30] R.A. Chevalier, C. Fransson, ApJ 420, 1994, 268-285.
[31] V.V. Dwarkadas, ApJ 630, 2005, 892-910.
[32] V.V. Dwarkadas, ApJ 667, 2007, 226-247.
[33] P. Blasi, et al., MNRAS 361, 2005, 907-918.